

The characteristic black hole mass resulting from direct collapse in the early universe

M. A. Latif,¹ D. R. G. Schleicher,¹ W. Schmidt,¹ J. C. Niemeyer¹

¹ Institut für Astrophysik, Georg-August-Universität,
Friedrich-Hund-Platz 1, D-37077 Göttingen, Germany

today

ABSTRACT

Black holes of a billion solar masses are observed in the infant universe a few hundred million years after the Big Bang. The direct collapse of protogalactic gas clouds in primordial halos with $T_{\text{vir}} \geq 10^4$ K provides the most promising way to assemble massive black holes. In this study, we aim to determine the characteristic mass scale of seed black holes and the time evolution of the accretion rates resulting from the direct collapse model. We explore the formation of supermassive black holes via cosmological large eddy simulations (LES) by employing sink particles and following their evolution for twenty thousand years after the formation of the first sink. As the resulting protostars were shown to have cool atmospheres in the presence of strong accretion, we assume here that UV feedback is negligible during this calculation. We confirm this result in a comparison run without sinks. Our findings show that black hole seeds with characteristic mass of $10^5 M_{\odot}$ are formed in the presence of strong Lyman Werner flux which leads to an isothermal collapse. The characteristic mass is about two times higher in LES compared to the implicit large eddy simulations (ILES). The accretion rates increase with time and reach a maximum value of $10 M_{\odot}/\text{yr}$ after 10^4 years. Our results show that the direct collapse model is clearly feasible as it provides the expected mass of the seed black holes.

Key words: methods: numerical – cosmology: theory – early Universe – galaxies: formation

1 INTRODUCTION

Black holes of a few millions to billions solar masses dwell in the center of present day galaxies (Kormendy & Richstone 1995; Tremaine et al. 2002; McConnell et al. 2011; van den Bosch et al. 2012). These supermassive black holes (SMBHs) are not only present in the local Universe but have been observed at $z > 6$ (Fan et al. 2003, 2006; Mortlock et al. 2011). Their formation in the first billions years after the Big Bang is still an open question.

Numerous models have been proposed to explain the origin and formation of supermassive black holes (Rees 1984; Regan & Haehnelt 2009a; Djorgovski et al. 2008; Begelman & Shlosman 2009; Regan & Haehnelt 2009b; Tanaka & Haiman 2009; Volonteri 2010; Haiman 2012; Johnson et al. 2012, 2013). They include the collapse of dense stellar cluster due to relativistic instability (Portegies Zwart et al. 2004; Omukai et al. 2008; Devecchi & Volonteri 2009), remnants of Population III stars (Haiman 2004) and the direct collapse of protogalactic gas clouds (Oh & Haiman 2002; Bromm & Loeb 2003; Spaans & Silk 2006; Begelman et al. 2006; Lodato & Natarajan 2006; Dijkstra et al. 2008; Djorgovski et al. 2008; Shang et al. 2010; Johnson et al. 2010; Schleicher et al. 2010; Latif et al. 2011; Choi et al. 2013; Whalen et al. 2013). Although, the formation of SMBHs from stellar mass black holes may appear as the most

natural way, the feedback from the stars creates a hindrance as they have to accrete at an Eddington rate all the time to reach the observed masses (Johnson & Bromm 2007; Alvarez et al. 2008; Whalen & Fryer 2012). The masses of black holes resulting from the collapse of dense stellar clusters are relatively low with $\sim 10^3 M_{\odot}$ (Devecchi & Volonteri 2009). On the other hand, the direct collapse seems the most plausible way to assemble SMBHs to provide higher mass black hole seeds.

The formation of SMBHs via direct collapse requires the suppression of fragmentation and efficient accretion of the gas onto the central object. Massive primordial halos of $10^7 - 10^8 M_{\odot}$ irradiated by strong Lyman Werner background fluxes are the most plausible candidates (Omukai 2001; Johnson & Bromm 2007; Dijkstra et al. 2008; Shang et al. 2010; Johnson et al. 2011; Schleicher et al. 2010; Wolcott-Green et al. 2011; Latif et al. 2011; Agarwal et al. 2012; Latif et al. 2013b), see also Inayoshi & Omukai (2012); Van Borm & Spaans (2013) for alternatives. Numerical simulations support this scenario and show that in the presence of strong Lyman Werner flux an isothermal collapse yields massive objects (Bromm & Loeb 2003; Wise et al. 2008; Regan & Haehnelt 2009c; Latif et al. 2011, 2013a). The final fate of these objects is not yet very well understood and depends on the gas mass accretion rates.

Theoretical models (Begelman et al. 2008; Begelman 2010;

Hosokawa et al. 2012; Schleicher et al. 2013; Whalen et al. 2013; Hosokawa et al. 2013) propose the formation of supermassive stars (normal stars of higher masses) or quasistars (stars with black holes at the center) as an intermediate stage to the formation of SMBHs. The work by Schleicher et al. (2013) suggests that for accretion rates $> 0.14 M_{\odot}/\text{yr}$, the core of the star collapses into a black hole, forming a so-called quasi-star while lower accretion rates lead to the formation of a supermassive star. Hosokawa et al. (2012, 2013) show that for accretion rates $> 10^{-2} M_{\odot}/\text{yr}$, supergiant stars of $10^5 M_{\odot}$ form via rapid accretion while maintaining the cool atmospheres on the Hayashi track. Schleicher et al. (2013) have suggested that this may be true up to a mass scale of $3.6 \times 10^8 \dot{m}^3 M_{\odot}$, where \dot{m} is the mass accretion rate in units of M_{\odot}/yr . These models for the evolution of supermassive stars show that in the presence of accretion rates $> 10^{-2} M_{\odot}/\text{yr}$, such stars have a bloated envelope and lower surface temperatures, inhibiting the emission of ionizing flux. A recent study by Latif et al. (2013a) reported high accretion rates of $1 M_{\odot}/\text{yr}$ in these halos and the possibility for the formation of massive objects in a short time.

In this article, we for the first time explore the characteristic mass scale of seed black holes and the time evolution of accretion rates in massive primordial halos illuminated by a strong Lyman Werner background UV flux. To accomplish this goal, we perform high resolution cosmological large eddy simulations to ensue the collapse below parsec scales by exploiting the adaptive mesh refinement method and employing sink particles to follow the accretion for longer time scales. To verify our results, we also perform a comparison run without sink particles. We evolve the simulations for twenty thousand years after the formation of the first sink and employ a Jeans resolution of 32 cells to resolve turbulent eddies. The subgrid-scale turbulence model of Schmidt et al. (2006) is used to take into account unresolved turbulence. This study will enable us to compute the masses of seed black holes formed in the massive primordial halos and test the feasibility of a direct collapse model.

This article is organized in the following way. In section 2, we describe the numerical methods and simulations setup. We present our results in section 3. In section 4, we summarize the main findings of this study and discuss our conclusions.

2 COMPUTATIONAL METHODS

2.1 Simulation Setup

The simulations presented here are performed using a modified version of the Enzo code (O’Shea et al. 2004; The Enzo Collaboration et al. 2013). Enzo is a Eulerian grid based, massively parallel, cosmological adaptive mesh refinement code. The hydrodynamical equations are solved using a 3rd order accurate piece-wise parabolic method (PPM). The dark matter dynamics is solved using the particle mesh technique.

The initial simulation setup is the same as in our previous study (Latif et al. 2013a). Here, we present a short summary of the initial conditions and the simulations setup. Our simulations are started with cosmological initial conditions at $z = 100$. We use the publicly available inits package to generate nested grid initial conditions. These simulations were first run with a uniform grid resolution of 128^3 and the dark matter haloes are selected at $z = 15$. The simulated volume has a comoving size of $1 \text{ Mpc } h^{-1}$ and the most massive halo lies at the center of the box. We further employ two initial nested refinements levels with a resolution of 128^3 cells each and initialize 5767168 particles to simulate the dark matter

dynamics. In the central 62 kpc region of the halo, we allow 15 dynamical refinement levels during the course of the simulations which yields an effective resolution of sub parsec scales (10,000 AU in comoving units). We resolve the Jeans length by 32 cells during the entire course of the simulations. Once the maximum refinement level is reached, we employ sink particles to follow the evolution for twenty thousand years after the formation of the first sink.

We employ a strong Lyman Werner flux of strength 10^3 in units of J_{21} produced by the first generation of stars with radiation spectra of 10^5 K (Omukai 2001; Johnson & Bromm 2007; Dijkstra et al. 2008; Schleicher et al. 2010; Wolcott-Green et al. 2011; Latif et al. 2011; Safranek-Shrader et al. 2012; Agarwal et al. 2012). To follow the thermal evolution, we self consistently solve the rate equations of H, H^+ , He, He^+ , He^{++} , e^- , H^- , H_2 , H_2^+ in the cosmological simulations. We ignore the effect of self-shielding as our main focus is on H_2 free halos.

To take into account the unresolved turbulence, we use the subgrid scale turbulence model proposed by Schmidt et al. (2006). The adaptively refined large eddy simulations technique is used to apply the SGS model in cosmological AMR simulations (Maier et al. 2009). We perform large eddy simulations (LES) and compare our results with implicit large eddy simulations (ILES). The approach of LES is based on scale separation mechanism i.e., separation of the resolved and unresolved scales, and connect them through an eddy-viscosity closure for the transfer of energy between the grid scales. The turbulent viscosity is computed from the grid scale and the SGS turbulence energy, i. e., the kinetic energy associated with numerically unresolved turbulent velocity fluctuations. On the other hand, ILES use only the numerical dissipation produced from the discretization errors of fluid dynamics equations.

In all, we have performed 6 simulations (3 LES, 3 ILES) with sink particles for three distinct halos A, B and C and a comparison run without sinks particles for halo A. The halo properties are given in the table 1 of Latif et al. (2013a). Their collapse redshifts are 12.6, 10.8 and 13.6 respectively. For a comparison run without sinks, simulations are evolved adiabatically after they reach the maximum refinement level. This method allows us to follow the collapse for a longer times.

2.2 Sink Particles

The need to resolve the Jeans length to stellar densities and Courant constraints on the calculation of the time step make it impossible to follow the collapse to the smallest scales while evolving the simulations for a long time. Therefore, sink particles are introduced to represent the gravitationally bound objects undergoing a free-fall collapse. This approach has been successfully employed in both SPH as well as in AMR codes (Bate et al. 1995; Krumholz et al. 2004; Federrath et al. 2010). Here, we employ the sink particle algorithm by Wang et al. (2010) to represent the protostars. Sinks are created when a grid cell is at the maximum refinement level, the density exceeds the Jeans density (i.e., it violates the Truelove criterion) and the overall flow is convergent, which is implicitly covered by a density threshold check. Furthermore, particles are merged if they are created within the accretion radius. The initial mass of the sinks is calculated such that the cell is Jeans stable after the subtraction of the sink mass. The initial velocity of the sinks is computed based on momentum conservation. Further details of the sinks algorithm can be found in the reference article (Wang et al. 2010).

The sink particles in our case do not accrete gas directly from

the grid as typically computed using the Bondi-Hoyle accretion. This effect is compensated by allowing the formation of additional sinks and subsequently, they are merged if they are formed within the accretion radius which we choose as the Jeans length. Using sink particles, we follow the collapse for longer dynamical time scales. This approach enables us to compute the masses of seed black holes and the time evolution of mass accretions.

3 MAIN RESULTS

3.1 Simulations with sink particles

We have performed 6 cosmological simulations with sink particles (3 LES and 3 ILES) for three distinct haloes A, B and C and employing a constant Lyman Werner background UV flux of $J_{21} = 10^3$ for stellar spectra of 10^5 K. We followed the evolution for twenty thousand years after the simulations reached the maximum refinement level and determined the characteristic mass scale of the most massive objects. The results obtained from the cosmological large eddy simulations are presented here. After the simulations are started at $z = 100$, massive halos are formed around redshift 18, and gas falls into the dark matter potentials and gets shock heated.

The general properties of the halos, twenty thousand years after the formation of the first sink are shown in figure 1. The formation of molecular hydrogen remains suppressed in the presence of strong H_2 photodissociating background and consequently, an isothermal collapse occurs. The central temperature of these halos is about 7000 K. The maximum density in the halos is a few times 10^{-18} g/cm³. There is an initial rise in the density at larger radii and then it becomes almost constant. This trend is observed for all halos. The deviation in the density radial profiles from an isothermal behavior may result both from the removal of the gas by sink particles from the grid as well as the formation of a disk due to the non-zero angular momentum. The typical radial velocities are a few km/s which indicate the relatively high gas infall rates at this stage of the collapse. The radial profile of the mass accretion rates shows that the accretion rate in the surroundings of the halo is about $1 M_\odot/\text{yr}$ and decreases down to $10^{-3} M_\odot/\text{yr}$ in the core of halo, the region which corresponds to the Jeans length. This behavior seems to be consistent for all halos. The ratio of rotational to circular velocities is about 1 in the surroundings of the halo and declines towards the center of the scale which corresponds to the Jeans length. It further shows that there is high degree of rotational support in the halo. The mass profiles increase with r^2 , the deviations from this behavior come from the differences in the underlying density structure for various runs.

The state of the simulations at their collapse redshift is shown in figure 2 and is presented by the density projections. The fragmentation in these halos remains suppressed and a single massive sink is formed in all haloes except one ILES run as discussed below. We note that the underlying density distribution is different from halo to halo for both LES and ILES. We attribute these differences to the properties of the halos and the occurrence of various processes such as the removal of gas by the sinks and turbulent stresses. We further show the time evolution of the density structure for the ILES run (halo C) in figure 3 where the formation of multiple sinks is observed. The formation of a second sink takes place about 7000 years after the formation of the first sink. The third sink particle in this case is formed about 10,000 years after the formation of the first sink. The mass of the most massive sink is about $10^5 M_\odot$. The masses of two particles are almost comparable

and may lead to a binary or even multiple system. Fragmentation in this halo is due to the local compression of the gas by the turbulence. Similarly, fragmentation was observed in our previous study (Latif et al. 2013a) with a different approach employed for the evolution of simulations. Here, no fragmentation is found in LES runs for all simulated halos.

The time evolution of the mass accretion rates for the most massive sinks is shown in figure 4 for both LES and ILES. The accretion rate increases with time and reaches a peak value of about 10 solar masses per year in about a time of a few thousand years. Such an accretion rate is in accordance with Bondi-Hoyle accretion

$$\dot{M} = \frac{4\pi\rho G^2 M^2}{c_s^3}. \quad (1)$$

Considering $M = 10^5 M_\odot$, $c_s = 12$ km/s and $\rho = 5 \times 10^{-19}$ g/cm³, the typical values in our case, the expected accretion rate from the above equation is $9.7 M_\odot/\text{yr}$ comparable to the values in our simulations. After about 10,000 years the accretion starts to become constant for LES. This time scale can be understood from the infall of a point mass m at distance R from a point source of mass M . The expression for the infall time can be derived from Kepler's third law of motion and is given as

$$T_{ff} = \frac{\pi}{2} \frac{R^{3/2}}{\sqrt{2G(M+m)}}. \quad (2)$$

For a point source of mass $10^5 M_\odot$ and a distance of 3×10^4 AU, the infall time is about 9,400 years and is in good agreement with our results. This characteristic behavior is noticed for all halos and for both LES and ILES runs. The decline in accretion rates after 10,000 years in one of the ILES runs is due to the formation of multiple sinks in halo C and a decrease in the density in the surroundings of the sink particle. The constant accretion rates after 10,000 years are a consequence of enhanced rotational support in the halo with time. The ratio of rotational to Keplerian velocity ($v_{\text{rot}}/v_{\text{cir}}$) increases with time as shown in figure 5. It indicates that as $v_{\text{rot}}/v_{\text{cir}}$ increases, it takes longer time for the gas to reach the center of the halo. It is further noted that LES runs lead to higher accretion rates compared to the ILES runs. We attribute the higher accretion rates (at least about a factor of 2 compared to ILES) in LES to the presence of an additional viscosity term. The occurrence of such high accretion rates has important implications for the evolution of supergiant stars. It is expected that in the presence of such high accretion rates the ionizing feedback from supermassive stars remains suppressed (Hosokawa et al. 2012; Schleicher et al. 2013).

As pointed out previously, our main aim here is to compute the characteristic mass scale of seed black holes resulting from the direct collapse model. The time evolution of the sink mass is shown in right panel of figure 4. The figure shows that sinks reach masses of $10^5 M_\odot$ in about a time of a few times 10^4 years. The masses of LES runs are higher (at least about a factor of 2) compared to the ILES runs. This is the consequence of the higher accretion rates in LES. It is found that a few percent of the halo mass goes into the sinks.

The mass distribution of the sinks for individual runs is illustrated in figure 6. It is clearly visible from the figure that LES runs produce higher mass sinks compared to the ILES runs. It can be noted that a single sink particle of $10^5 M_\odot$ is formed per halo except for halo C which has two additional particles of about $5 \times 10^4 M_\odot$ and $8 \times 10^4 M_\odot$.

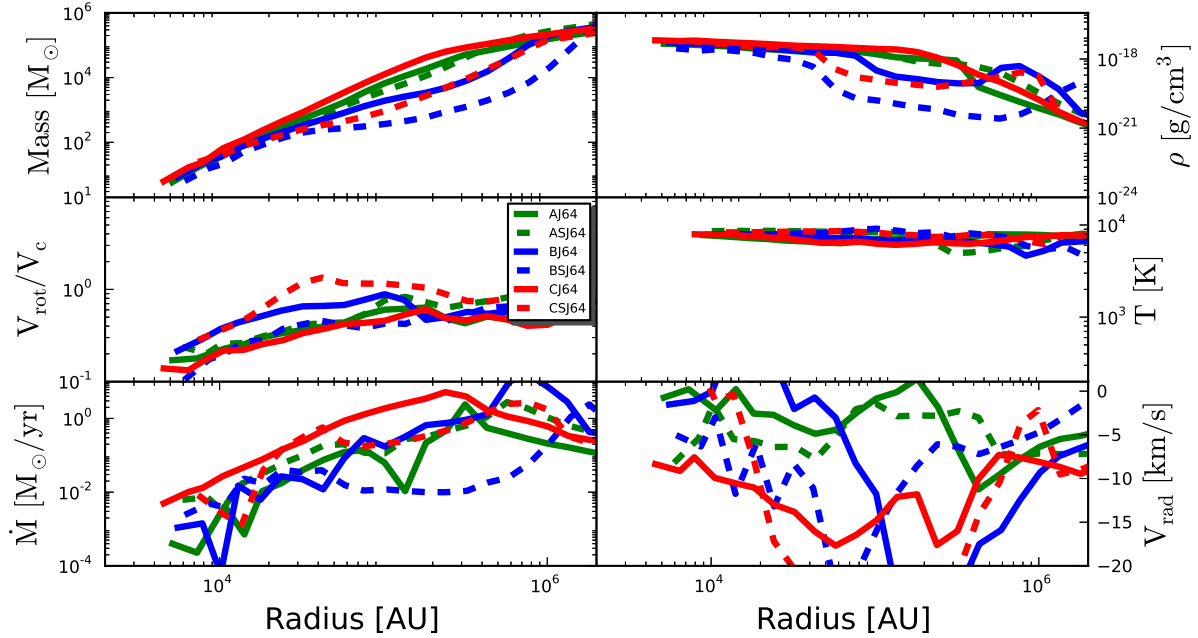


Figure 1. Radially binned spherically averaged radial profiles are shown for the halos A, B and C. The solid lines represent ILES runs while the dashed lines stand for LES runs. Top left and right panels show the enclosed mass and density radial profiles. The rotational velocity and temperature radial profiles are depicted in the middle left and right panels. The bottom panels show accretion rates and radial velocity profiles.

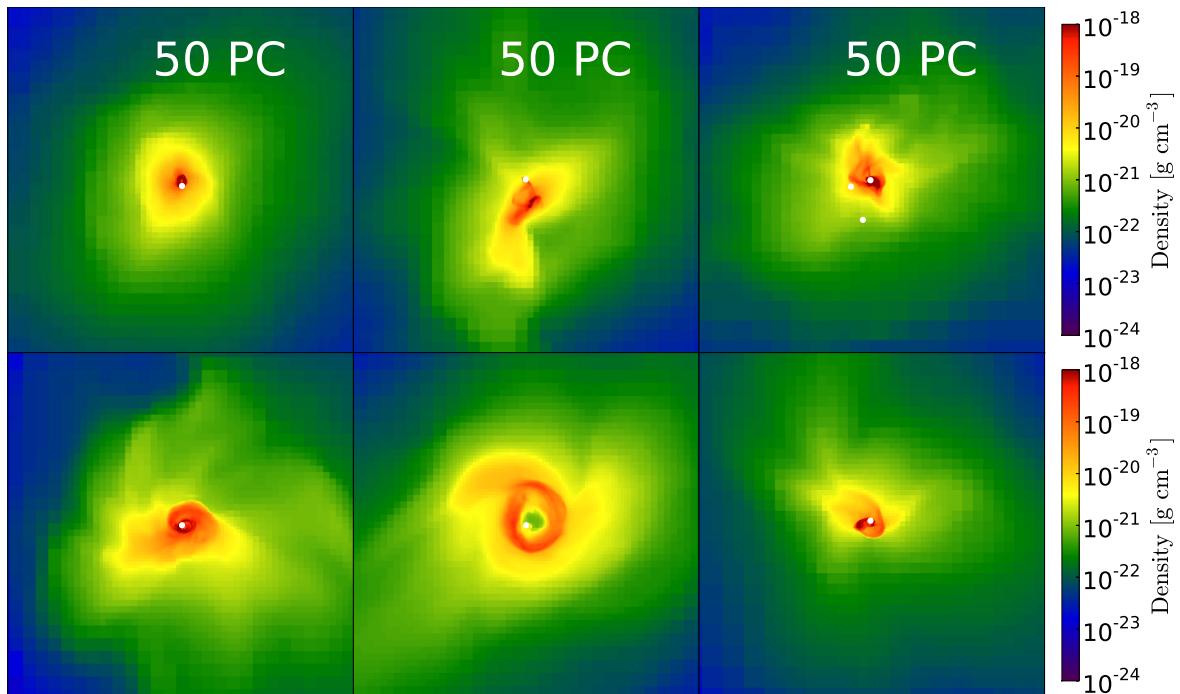


Figure 2. Density projections are shown for the central 50 pc twenty thousand years after the formation of the first sink. The white spheres represent sink particles and are overlotted on the density projections. They have typical masses of $\sim 10^5 M_\odot$.

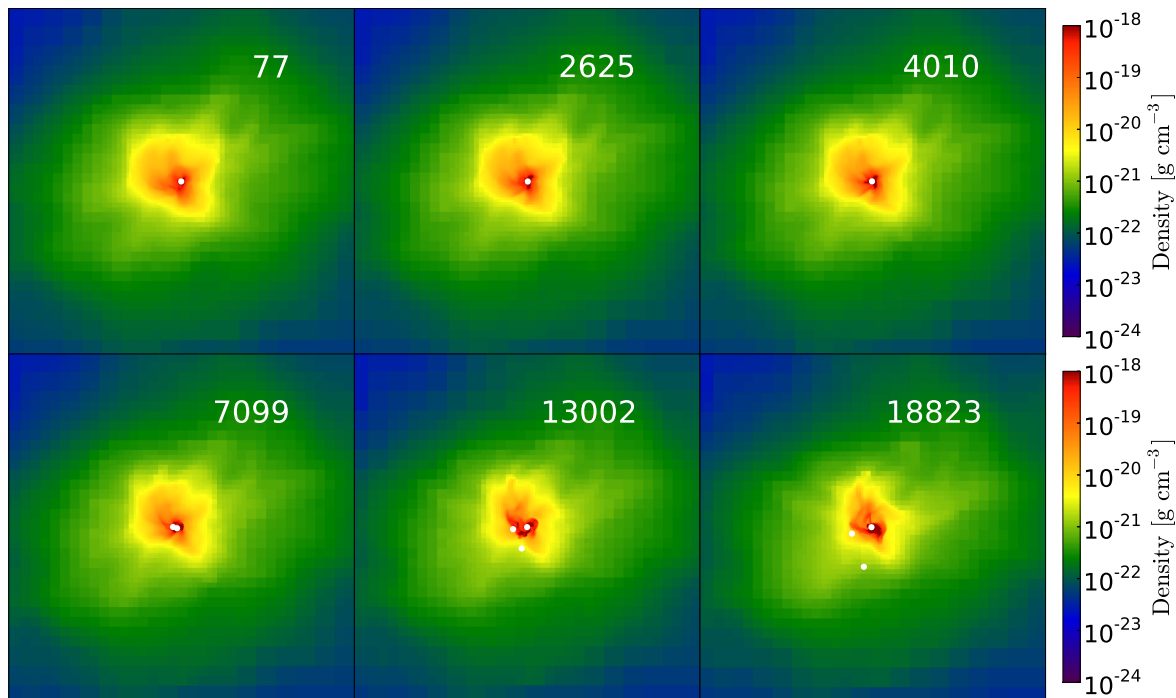


Figure 3. Time evolution of the density projections is shown in this figure for an ILES run (halo C). The time in years, after the formation of the first sink is shown in each projection. The white spheres represent sink particles and are overlotted on the density projections. They have typical masses of $\geq 10^4 M_\odot$.

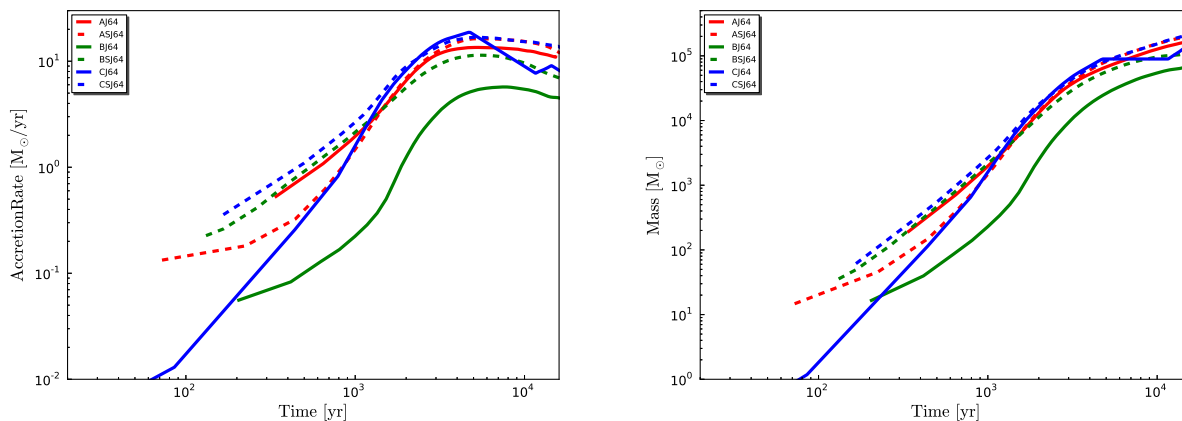


Figure 4. Time evolution of the accretion rates on the most massive sinks is shown in the left panel of this figure. The time evolution of the masses of the most massive sinks is depicted in the right panel. The solid lines represent ILES runs while dashed lines stand for LES runs.

3.2 Comparison run without sinks

In addition to our 6 cosmological runs with sink particles, we have performed one cosmological simulation where we evolve the simulation adiabatically at densities above a few times 10^{-18} g/cm^3 after reaching the maximum refinement level. The properties of the halo are shown in figure 7 after 20,000 years of evolution. The density radial profile shows an isothermal behavior at larger radii and becomes almost flat in the center due to the adiabatic evolution. The temperature is about 8000 K and starts to increase with density to make the collapse stable at the smallest scales. The radial infall velocity is about 10 km/s and becomes almost constant in the center. The mass accretion rate is about $1 M_\odot/\text{yr}$ as collapse proceeds on the larger scales and decreases down to the $10^{-4} M_\odot/\text{yr}$ within the Jeans length. The rotational velocity is low in the center, peaks

around 10^5 AU and declines down as it follows the Keplerian velocity. The mass radial profiles increase with r^2 in the center and becomes flat at larger radii. This indicates that most of the mass lies in the central clump.

The state of the simulations after twenty thousand years of the evolution is shown in figure 8. It is clearly visible from the density projections that a disk is formed in the center of the halo. The mass of the disk is $\sim 10^5 M_\odot$ equivalent to the sink mass in the corresponding run. The formation of a parsec size disk is according to the expectation of theoretical models for the black hole formation (Lodato & Natarajan 2006). Both approaches provide high masses in relatively short time scales. This verification of results without sinks puts our estimates on even sounder footing.

We further show the time evolution of the mass radial profile

for this run as depicted in the left panel of figure 9. It can be noticed that initially the mass follows an r^2 behavior within the Jeans length and then increases linearly with radius. This trend is consistent with an isothermal density profile. Over the passage of time, the mass increases due to the infall of gas in the center of the halo and profile gets flattened. A disk of $\sim 10^5 M_\odot$ is formed and most of the mass lies in the central clump as indicated by the flat mass profile. The time evolution of the accretion rates radial profile is shown in the right panel of figure 9. Similar to sinks simulation, accretion rate increases with time and reaches a few solar masses per year in about 10,000 years. We note that the accretion rate measured here effectively probes a larger scale, and the profiles indicate an increase towards smaller scales. We therefore consider them to be consistent with sink particle runs.

4 DISCUSSION

We present here the results from the first cosmological large eddy simulations employing sink particles and following the collapse for 20,000 years after their formation. These simulations are performed for three distinct halos and the results are compared with implicit large eddy simulations. The main objective of this study is to compute the characteristic mass scale of seed black holes resulting from the direct collapse model. We also computed the time evolution of mass accretion rates in massive primordial halos irradiated by a strong Lyman Werner UV background flux.

Our findings show that black hole seeds with characteristic masses of $10^5 M_\odot$ are formed in a short time scale of twenty thousand years after their formation. It is further found that the characteristic masses are two times higher in LES. The time evolution of the accretion rates shows a characteristic behavior, it increases with time and reaches a peak value of $10 M_\odot/\text{yr}$. The accretion rate becomes almost constant as the rotational support is increased in the halo at later times. We further noticed that multiple sinks are formed in one halo with masses between $5 \times 10^4 - 10^5 M_\odot$. It is worth mentioning that we confirmed our estimates for the masses of sinks by evolving simulations adiabatically soon after they reached the maximum refinement level (an alternative approach to sinks) and found similar results. We further stress that our estimates for the characteristic mass are robust as they are confirmed from two independent approaches.

The results from this study suggest that the formation of supermassive stars of $10^5 M_\odot$ seems the most plausible outcome as an intermediate stage to the formation of supermassive black holes. This is in accordance with the prediction of theoretical studies (Begelman 2010; Hosokawa et al. 2012; Schleicher et al. 2013; Hosokawa et al. 2013). We have further shown that higher accretion rates of $\geq 0.1 M_\odot/\text{yr}$ can be maintained for longer time scales. Our simulations show that SGS turbulence favors higher accretion rates compared to the ILES and the resulting seed black holes are about two times more massive.

It is expected that supermassive protostars produce accretion luminosity feedback during their early stage. Our calculations did not take into account this effect. We expect that the accretion luminosity feedback will have only minor impact on the masses of seed black holes as similar study exploring this impact in minihalos reported no significant impact (Smith et al. 2011, 2012). The UV feedback is expected to occur when the star mass exceeds $10^5 M_\odot$ (Hosokawa et al. 2013) which may further influence the growth of such stars (Hosokawa et al. 2012; Johnson et al. 2012). Numerical

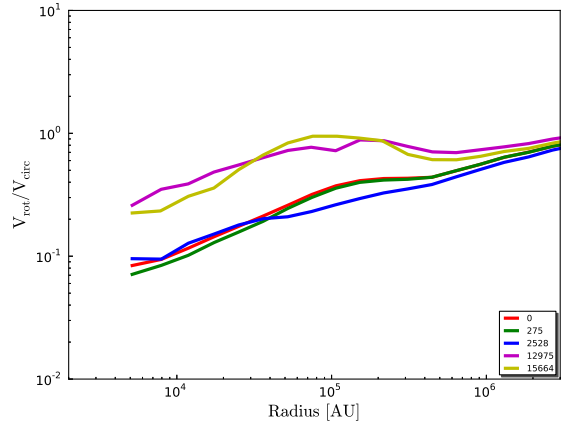


Figure 5. The time evolution of the ratio of rotational to Kepler velocity as a function of radius is shown in the figure. The time corresponding to each profiles is shown in the legend and its units are in years.

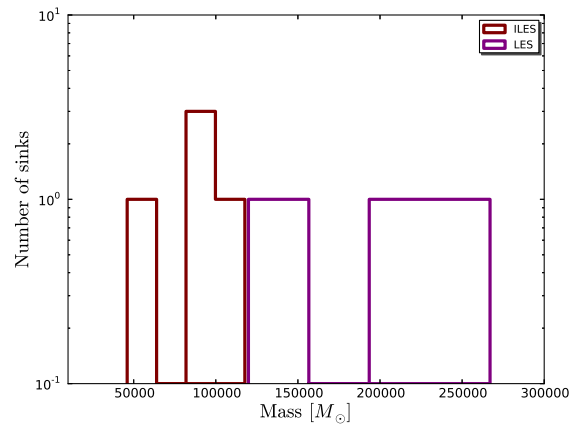


Figure 6. Mass distribution of the sinks is shown in this figure. The purple color shows the sink mass distribution for the LES runs while brown color represents ILES runs.

simulations exploring the impact of UV feedback should be performed in the future.

ACKNOWLEDGMENTS

The simulations described in this work were performed using the Enzo code, developed by the Laboratory for Computational Astrophysics at the University of California in San Diego (<http://lca.ucsd.edu>). We acknowledge research funding by Deutsche Forschungsgemeinschaft (DFG) under grant SFB 963/1, projects A12, A15 and computing time from HLRN under project nip00029. DRGS thanks the DFG for funding via the Schwerpunktprogram SPP 1573 “Physics of the Interstellar Medium” (grant SCHL 1964/1 – 1). The simulation results are analyzed using the visualization toolkit for astrophysical data YT (Turk et al. 2011).

REFERENCES

Agarwal B., Khochfar S., Johnson J. L., Neistein E., Dalla Vecchia

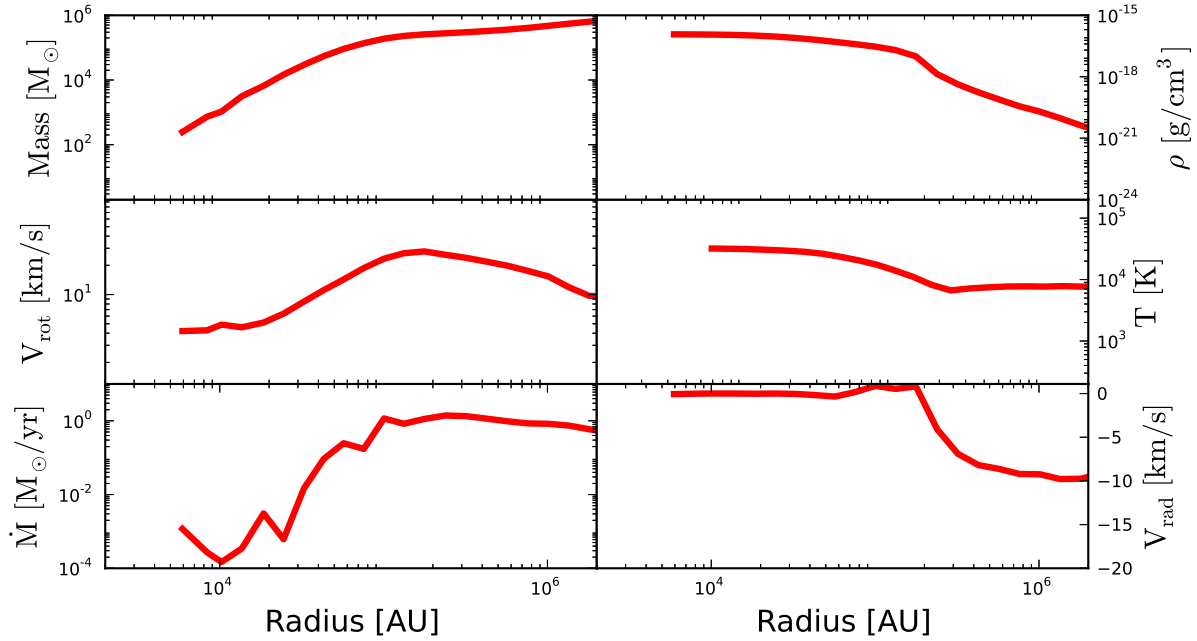


Figure 7. Radially binned spherically averaged radial profiles are shown for the run without sinks (for halo A). The radial profiles of the enclosed mass and the density are shown in the top left and right panels. The middle left panel shows the rotational velocity profile while the right middle panel depicts the temperature radial profiles. The bottom panels show the mass accretion rate and radial velocity profiles.

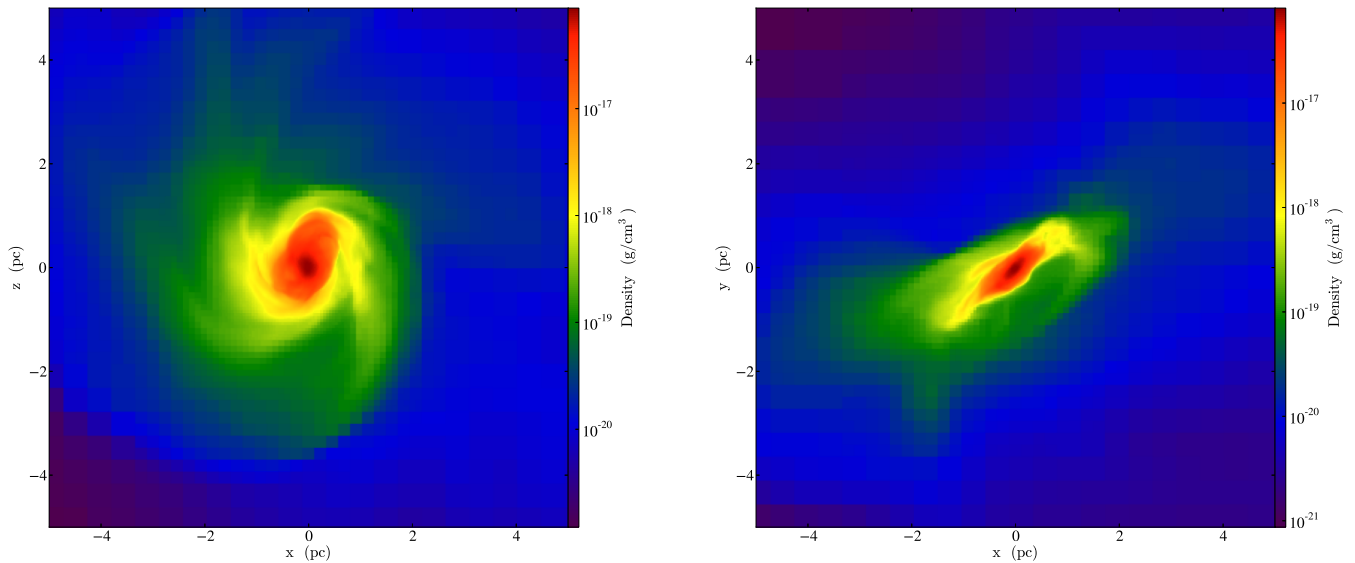


Figure 8. Density projections are shown for the central 10 pc for the run without sinks. The left and right panels show the projections along the y - and z -axis.

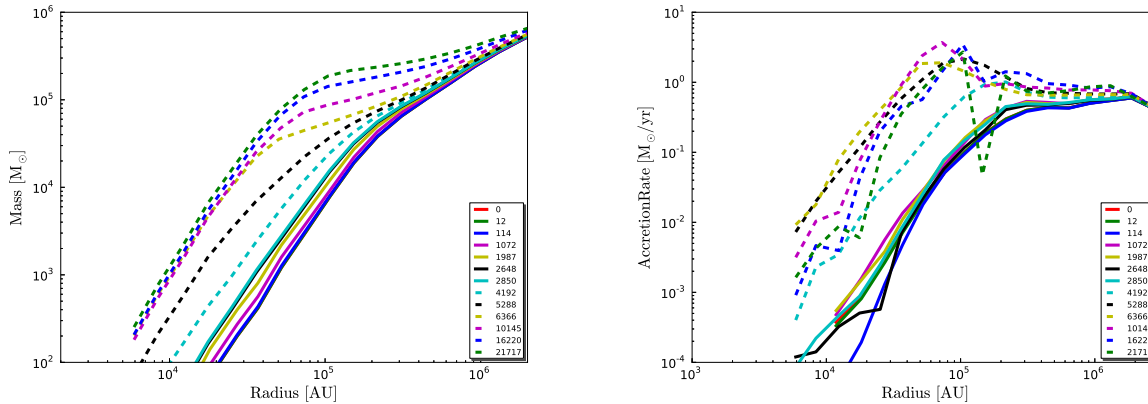


Figure 9. Time evolution of the mass and accretion rate radial profiles for the run without sinks. The left panel shows the mass radial profiles and the right panel shows the accretion rate radial profiles. The time corresponding to each radial profile is shown in the legend and its units are in years.

C., Livio M., 2012, MNRAS, 425, 2854

Alvarez M. A., Wise J. H., Abel T., 2008, ArXiv e-prints-0811.0820

Bate M. R., Bonnell I. A., Price N. M., 1995, MNRAS, 277, 362

Begelman M. C., 2010, MNRAS, 402, 673

Begelman M. C., Rossi E. M., Armitage P. J., 2008, MNRAS, 387, 1649

Begelman M. C., Shlosman I., 2009, ApJ, 702, L5

Begelman M. C., Volonteri M., Rees M. J., 2006, MNRAS, 370, 289

Bromm V., Loeb A., 2003, ApJ, 596, 34

Choi J.-H., Shlosman I., Begelman M. C., 2013, ArXiv e-prints-1304.1369

Devecchi B., Volonteri M., 2009, ApJ, 694, 302

Dijkstra M., Haiman Z., Mesinger A., Wyithe J. S. B., 2008, MNRAS, 391, 1961

Djorgovski S. G., Volonteri M., Springel V., Bromm V., Meylan G., 2008, ArXiv e-prints-0803.2862

Fan X., Strauss M. A., Richards G. T., Hennawi J. F., Becker R. H., White R. L., Diamond-Stanic A. M., 2006, AJ, 131, 1203

Fan X., Strauss M. A., Schneider D. P., Becker R. H., White R. L., Haiman Z., Gregg M., 2003, AJ, 125, 1649

Federrath C., Banerjee R., Clark P. C., Klessen R. S., 2010, ApJ, 713, 269

Haiman Z., 2004, ApJ, 613, 36

Haiman Z., 2012, ArXiv e-prints-1203.6075

Hosokawa T., Omukai K., Yorke H. W., 2012, ApJ, 756, 93

Hosokawa T., Yorke H. W., Inayoshi K., Omukai K., Yoshida N., 2013, ArXiv e-prints:1308.4457

Inayoshi K., Omukai K., 2012, MNRAS, 422, 2539

Johnson J. L., Bromm V., 2007, MNRAS, 374, 1557

Johnson J. L., Khochfar S., Greif T. H., Durier F., 2010, MNRAS, pp 1427–+

Johnson J. L., Khochfar S., Greif T. H., Durier F., 2011, MNRAS, 410, 919

Johnson J. L., Whalen D. J., Fryer C. L., Li H., 2012, ApJ, 750, 66

Johnson J. L., Whalen D. J., Li H., Holz D. E., 2013, ApJ, 771, 116

Kormendy J., Richstone D., 1995, ARA&A, 33, 581

Krumholz M. R., McKee C. F., Klein R. I., 2004, ApJ, 611, 399

Latif M. A., Schleicher D. R. G., Schmidt W., Niemeyer J., 2013a, MNRAS, 433, 1607

Latif M. A., Schleicher D. R. G., Schmidt W., Niemeyer J., 2013b, MNRAS, p. 551

Latif M. A., Schleicher D. R. G., Spaans M., Zaroubi S., 2011, A&A, 532, A66

Latif M. A., Zaroubi S., Spaans M., 2011, MNRAS, 411, 1659

Lodato G., Natarajan P., 2006, MNRAS, 371, 1813

Maier A., Iapichino L., Schmidt W., Niemeyer J. C., 2009, ApJ, 707, 40

McConnell N. J., Ma C.-P., Gebhardt K., Wright S. A., Murphy J. D., Lauer T. R., Graham J. R., Richstone D. O., 2011, Nature, 480, 215

Mortlock D. J., Warren S. J., Venemans B. P., Patel M., Hewett P. C., McMahon R. G., Simpson C., Theuns T., González-Solares E. A., Adamson A., Dye S., Hambly N. C., Hirst P., Irwin M. J., Kuiper E., Lawrence A., Röttgering H. J. A., 2011, Nature, 474, 616

Oh S. P., Haiman Z., 2002, ApJ, 569, 558

Omukai K., 2001, ApJ, 546, 635

Omukai K., Schneider R., Haiman Z., 2008, ApJ, 686, 801

O’Shea B. W., Bryan G., Bordner J., Norman M. L., Abel T., Harkness R., Kritsuk A., 2004, ArXiv Astrophysics e-prints 0403044

Portegies Zwart S. F., Baumgardt H., Hut P., Makino J., McMillan S. L. W., 2004, Nature, 428, 724

Rees M. J., 1984, ARA&A, 22, 471

Regan J. A., Haehnelt M. G., 2009a, MNRAS, pp 640–+

Regan J. A., Haehnelt M. G., 2009b, MNRAS, 396, 343

Regan J. A., Haehnelt M. G., 2009c, MNRAS, 393, 858

Safrank-Shrader C., Agarwal M., Federrath C., Dubej A., Milosavljević M., Bromm V., 2012, MNRAS, 426, 1159

Schleicher D. R. G., Palla F., Ferrara A., Galli D., Latif M., 2013, ArXiv e-prints-1305.5923

Schleicher D. R. G., Spaans M., Glover S. C. O., 2010, ApJ, 712, L69

Schmidt W., Niemeyer J. C., Hillebrandt W., 2006, A&A, 450, 265

Shang C., Bryan G. L., Haiman Z., 2010, MNRAS, 402, 1249

Smith R. J., Glover S. C. O., Clark P. C., Greif T., Klessen R. S., 2011, MNRAS, 414, 3633

Smith R. J., Hosokawa T., Omukai K., Glover S. C. O., Klessen R. S., 2012, MNRAS, 424, 457

Spaans M., Silk J., 2006, ApJ, 652, 902

Tanaka T., Haiman Z., 2009, ApJ, 696, 1798

- The Enzo Collaboration Bryan G. L., Norman M. L., O'Shea B. W., Abel T., Wise J. H., Turk M. J., Reynolds D. R., Collins D. C., Wang P., Skillman S. W., 2013, ArXiv e-prints
- Tremaine S., Gebhardt K., Bender R., Bower G., Dressler A., Faber S. M., Filippenko A. V., Green R., Grillmair C., Ho L. C., Kormendy J., Lauer T. R., Magorrian J., Pinkney J., Richstone D., 2002, ApJ, 574, 740
- Turk M. J., Smith B. D., Oishi J. S., Skory S., Skillman S. W., Abel T., Norman M. L., 2011, ApJS, 192, 9
- Van Borm C., Spaans M., 2013, A&A, 553, L9
- van den Bosch R. C. E., Gebhardt K., Gültekin K., van de Ven G., van der Wel A., Walsh J. L., 2012, Nature, 491, 729
- Volonteri M., 2010, A&A Rev., 18, 279
- Wang P., Li Z.-Y., Abel T., Nakamura F., 2010, ApJ, 709, 27
- Whalen D. J., Even W., Lovekin C. C., Fryer C. L., Stiavelli M., Roming P. W. A., Cooke J., Pritchard T. A., Holz D. E., Knight C., 2013, ApJ, 768, 195
- Whalen D. J., Fryer C. L., 2012, ApJ, 756, L19
- Whalen D. J., Johnson J. L., Smidt J., Meiksin A., Heger A., Even W., Fryer C. L., 2013, ApJ, 774, 64
- Wise J. H., Turk M. J., Abel T., 2008, ApJ, 682, 745
- Wolcott-Green J., Haiman Z., Bryan G. L., 2011, MNRAS, 418, 838